JOURNAL OF PROPULSION AND POWER
Vol. 17, No. 4, July–August 2001

Nonlinear Dynamic Combustion in Solid Rockets: L^* Effects

K. C. Tang* M. Q. Brewster†
University of Illinois at Urbana–Champaign, Urbana, Illinois 61801

Nonlinear combustion and bulk-mode (L^*) chamber gasdynamics in homogeneous solid propellant rockets are simulated computationally. A relatively new nonlinear simplified-kinetics combustion model is used. Quasi-steady gas and surface decomposition are assumed. Linear, oscillatory analytical results are recovered (as numerical validation). In general, the calculated results exhibit motor behavior in agreement with that observed experimentally for different L^* values, as summarized by Price (Price, E. W., "L^* Instability," *Nonsteady Burning and Combustion Stability of Solid Propellants*, edited by L. De Luca, E. W. Price, and M. Summerfield, Vol. 143, Progress in Astronautics and Aeronautics, AIAA, Washington, DC, 1992, Chap. 9, pp. 325–361) increases from low, $<L_0^*$, to high, $>L_0^*$, values burning rate and motor pressure go from erratic and/or oscillatory to steady and stable. Several nonlinear combustion phenomena that have been observed experimentally but that are beyond the capability of linearized models are also predicted. These include rapid initial (over-) pressurization, propellant extinction, and dual-frequency and limit-cycle oscillations. The results suggest that some of these combustion phenomena could be due to nonlinear (but still quasi-steady) dynamic burning and mass conservation effects within the classical bulk-mode framework rather than more complicated fluid and flame dynamic effects that have been proposed. In particular, the rapid rate of initial pressurization and the ignition spike commonly attributed to erosive burning may be due to nonlinear dynamic burning at low L^*. Even without an overpressurization spike, it appears that the rapid pressurization rate in solid rockets is at least partly due to the inherent L^* instability of the initial state where $L^* < L_0^*(\alpha > 0)$ because of large values of L_0^* at low pressures.

Nomenclature

A = $(\bar{T}_s - T_0)(\partial \ln \bar{m}/\partial \bar{T}_s)_p$, k/r
A' = $1/(RT_f C_d)$
A_b = burning area
A_c = condensed-phase reaction rate prefactor
A_t = nozzle throat area
B = $1/[(\bar{T}_s - T_0)(\partial \ln \bar{m}/\partial T_0)p]$, $1/k$
B_g = gas-phase reaction rate prefactor
C = specific heat, C_p
C_d = isentropic nozzle discharge coefficient
E_c = activation energy of condensed-phase reaction
E_g = activation energy of gas-phase reaction
$F_{c,g}$ = functions generated by flame models
f = frequency, Hz
f_s = temperature gradient at surface in condensed phase
k = $(\bar{T}_s - T_0)(\partial \ln \bar{m}/\partial T_0)_p$
$k_{c,g}$ = thermal conductivity
L^* = characteristic length, V/A_t
m = mass flux, $\rho_c r_b$
m' = $\Delta m \exp[i(2\pi f t + \Theta)]$
n = $(\partial \ln \bar{m}/\partial \ln \bar{P})_{T_0}$, ν
n_s = $(\partial \ln \bar{m}/\partial \ln \bar{P})_{T_s}$, δ/r
P = pressure
P' = $\Delta P \exp[i 2\pi f t]$
$Q_{c,g}$ = heat release (positive exothermic)
q_c = conductive heat flux to surface from gas phase
R = universal gas constant, 1.987 cal/mol · K
R_p = pressure-driven frequency-response function, $(m'/\bar{m})/(P'/\bar{P})$
r = $(\partial \bar{T}_s/\partial T_0)_p$
r_b = burning rate
T = temperature
T_{0a} = parameter defined by Eq. (10)
$T_{0,s,f}$ = initial, surface, or final flame temperature
t = time
V = free combustion chamber volume
W = molecular weight
x = coordinate normal to surface, positive into gas phase
x_c = solid convective–diffusive length scale, $\alpha_c/\bar{r}_b$
α = linear acoustic oscillation growth/damping parameter
$\alpha_{c,g}$ = thermal diffusivity
Δ = amplitude of fluctuating quantity
δ = Jacobian parameter, $\nu r - \mu k$
Θ = phase angle of burning rate oscillation relative to pressure oscillation
λ = $\frac{1}{2} + (\frac{1}{2})(1 + 4i\Omega)^{1/2}$
ν = $(\partial \ln \bar{m}/\partial \ln \bar{P})_{T_0}$, n
$\rho_{c,g}$ = density
τ_{ch} = combustor relaxation time
ω = $2\pi f$

Subscripts and Superscripts

c = condensed phase, convective–diffusive, or conduction
f = flame
g = gas phase
s = surface
0 = initial condition or $\alpha = 0$
$\bar{}$ = steady condition or mean value
$'$ = complex fluctuating quantity

Introduction

THE simplest mode of coupling between motor fluid dynamics and propellant combustion in solid rockets is the bulk mode. In this mode, transient burning is coupled with spatially uniform (nonacoustic) pressure variations in the motor.[1–13] Under certain conditions, this coupling can lead to unstable combustor operation, usually identified by oscillatory pressure variations. Sometimes these oscillatory motions lead to extinction or quenching of the propellant. L^* instability, as it is usually called, is so named because L^* has been found to be a key parameter in determining the system

Received 16 June 2000; revision received 15 March 2001; accepted for publication 30 March 2001.

*Research Programmer, Center for Simulation of Advanced Rockets.
†Professor of Mechanical Engineering, Department of Mechanical and Industrial Engineering.

behavior, where L^* is defined as the free chamber volume-to-nozzle throat area ratio ($L^* = V/A_t$). Motors susceptible to this type of instability are typically those with low L^* values, for example, small motors with high propellant volume loading (small V) operating at low pressures (large A_t). Because most motors are not susceptible to oscillatory L^* instability, it has not been studied as extensively as acoustic instability, velocity coupling, or other fluid dynamic effects that are suspected of playing a role in undesirable motor behavior. Nevertheless, as argued by Price,[1,2] and others, the bulk mode of unsteady motions is still a useful one for studying propellant combustion behavior. It is of particular interest for studying the relatively uncharted area of nonlinear, coupled solid propellant combustion–gasdynamic behavior because it represents the simplest mode of such coupling. Furthermore, it appears that combustor instability at low L^* might be a much more important factor in interior ballistics than has generally been recognized. Virtually every motor goes through a process of trying to make a transition from a highly unstable initial state to a stable operating state or manifold of states. As demonstrated in this paper, the success of this transition depends critically on nonlinear combustion and L^*-combustor dynamics.

The basic mechanism of bulk-mode oscillations at low L^* is coupling between combustion of the solid propellant and bulk-mode filling and emptying of the gas-filled port or motor chamber. The frequencies normally associated with low-L^* oscillations are of the order of 100 Hz or less, being determined by the chamber residence time and combustion properties of the burning propellant. The primary time-lag process of importance with respect to combustion is thermal conduction in the heated surface layer of the burning solid. Transient thermal relaxation in the solid affects the temperature profile near the burning surface. This in turn affects the high-activation-energy decomposition process near the surface and, therefore, the burning rate. The pressure-sensitive process that is mainly responsible for coupling combustion to chamber gas motions is gas-phase flame kinetics, which is generally taken to be quasi–steady. Thus, perturbations in chamber pressure produce fluctuations in burning rate via combustion processes, and conversely, fluctuations in burning rate produce perturbations in pressure via chamber mass conservation; the system is coupled. Because fluctuations in burning rate and pressure are always present naturally during a motor firing (through propellant nonhomogeneity, particles and debris passing through the nozzle, and viscous fluid mechanical effects), there is the possibility, if conditions are right, that these perturbations can grow in amplitude. Whether these perturbations grow or decay and at what rate and frequency are questions that can be and have been addressed relatively successfully by linear theory, at least for homogeneous propellants. Nonlinear behavior, however, has not been so successfully described theoretically.

Several nonlinear behaviors have been observed in solid rocket motors (see the left side of Fig. 1, which is Price's[1] summary of experimental observations). Figure 1a shows a case where the motor reaches a linearly stable state at elevated pressure such that small-amplitude perturbations always damp. Other times, as shown in Fig. 1b, oscillations have been observed to grow exponentially in amplitude and then converge to a stable state. Sometimes, particularly in low-L^* motors with L^* slightly smaller than the critical value at the stability boundary (linear growth constant α positive but small), these oscillations grow to large amplitude followed by sudden extinction or quenching of propellant combustion. In some cases extinction is followed by spontaneous reignition and additional cycles of quenching and ignition, called chuffing (Fig. 1c). For motors with even smaller L^* values (α positive and large), the amplitude growth rate is so large that no oscillation is possible before extinction occurs (Fig. 1d). In addition, it has been observed[6–10] that during a single motor firing two different oscillations with different frequencies can occur, so-called dual-frequency oscillations or frequency shifting. In double-base propellants this behavior has been tentatively attributed to non-quasi-steady, multistage gas flame dynamics[6,7] (incomplete combustion), although no theoretical–experimental comparison has yet established this explanation. Price[1] has also suggested a quasi-linear explanation for dual-frequency behavior in terms of multiple-valued frequencies for a single L^* value within a narrow parameter space of linear response function parameters. Thus, a variety of nonlinear bulk-mode behaviors have been recognized as such, but have not yet been adequately described theoretically.

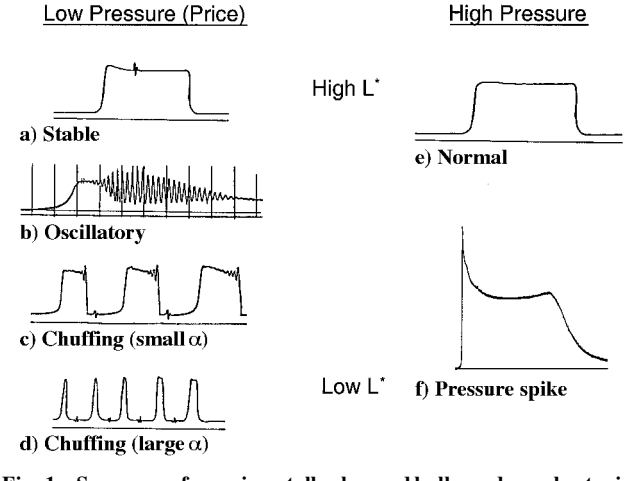

Fig. 1 Summary of experimentally observed bulk-mode combustor instability for various values of L^* (left side from Price[1]).

There are also nonlinear motor phenomena attributed to other factors when they are or may be actually manifestations of combustor and combustion dynamics at low L^*. Price[2] has observed that chuffing being interpreted as an ignition problem is a common misdiagnosis under low-L^* and low-pressure conditions. The results of the present investigation have led us to propose one other potential common misdiagnosis: that the initial overpressurization spike sometimes experienced in small motors, which is often attributed to erosive burning or igniter mass flux, may actually be primarily simple bulk-mode combustor dynamics due to low L^* (see Fig. 1f). Both low-L^* combustor dynamics and erosive burning would be expected to occur in similar kinds of motor geometries and could, therefore, easily be mistaken. The reasons the initial pressurization spike has not been more widely recognized as a dynamic burning effect may have to do with the general lack of sufficiently accurate, nonlinear, time-dependent combustion models, as well as other factors.

This paper describes a computational investigation of nonlinear bulk-mode combustor and combustion dynamics using a combustion model developed by Ward et al.[14] (WSB in the following) that has recently shown promise for simulating linear dynamic combustion behavior of homogeneous energetic materials (nitrocellulose/nitroglycerin and cyclotetramethylene tetranitramine). The framework of the combustion analysis is the classical quasi-steady, homogeneous, one-dimensional (QSHOD) theory. The combustion model is coupled with a simple combustion chamber and quasi-steady, isentropic nozzle. Acoustic motions in the gas chamber are not considered. The time-dependent pressure and propellant burning rate are solved numerically via the coupled nonlinear equations for conservation of mass in the chamber and energy in the solid propellant. The equations, though straightforward and documented elsewhere, are summarized in the following section for those unfamiliar with this type of analysis.

Numerical Modeling

Nonlinear Combustion Model

The theory of Zeldovich and Novozhilov (ZN) is used in combination with the WSB flame modeling (FM) approach for the nonlinear combustion model. Details of the derivation can be found in Refs. 15–17. QSHOD conditions are assumed for the propellant and flame zone. The fundamental equation for QSHOD propellant combustion is the unsteady energy equation in the condensed phase, which includes the inert solid propellant ($-\infty < x < 0$) and the thin (possibly liquid) decomposition layer on the propellant surface ($x = 0$):

$$\rho_c C \frac{\partial T}{\partial t} + mC \frac{\partial T}{\partial x} = k_c \frac{\partial^2 T}{\partial x^2} \tag{1}$$

$$T(-\infty, t) = T_0 \tag{1a}$$

$$T(0, t) = T_s(t) \tag{1b}$$

$$\left.\frac{\partial T}{\partial x}\right|_{0^-,t} \equiv f_s(t) = \frac{1}{k_c}(q_c + mQ_c), \qquad q_c = k_g \left.\frac{\partial T}{\partial x}\right|_{0^+,t} \tag{1c}$$

The solution of the unsteady heat equation is a relatively straightforward matter, even when, in addition to solid temperature, $T(x, t)$, the burning mass flux, $m(t) = \rho_c r_b(t)$, is an unknown eigenvalue to be solved for. What complicates the solution is the question of how to specify the conductive heat feedback to the surface from the gas phase. One approach is to solve gas-phase quasi-steady differential equations, based on some kinetics assumptions (usually single step), as in the FM approach. The ZN method provides a convenient alternative for representing the conductive heat feedback from the quasi-steady gas phase instead of solving the quasi-steady gas equations. The method consists of using the steady burning laws and integral energy equations to transform the steady burning laws to a form that is valid for unsteady burning. The steady burning laws can be represented functionally as

$$\bar{m} = \bar{m}(T_0, \bar{P}) \tag{2}$$

$$\bar{T}_s = \bar{T}_s(T_0, \bar{P}) \tag{3}$$

where the indicated functionalities can be either in the form of analytic flame modeling equations (FM approach) or empirical data (ZN approach). (An overbar represents time-independent or time-mean conditions.) Using the steady integral energy equation

$$\bar{f}_s = (\bar{r}_b/\alpha_c)(\bar{T}_s - T_0) \tag{4}$$

the steady burning laws can be transformed to eliminate T_0 in favor of $\bar{f}_s$:

$$\bar{m} = \bar{m}(\bar{f}_s, \bar{P}) \tag{5}$$

$$\bar{T}_s = \bar{T}_s(\bar{f}_s, \bar{P}) \tag{6}$$

These functional relationships have been shown to be valid on a time-dependent basis[15,16] under the quasi-steady assumption, giving

$$m = m(f_s, P) \tag{7}$$

$$T_s = T_s(f_s, P) \tag{8}$$

With the use of the time-dependent integral energy equation, assuming surface reaction,

$$f_s = \frac{r_b}{\alpha_c}\left(T_s - \left[T_0 - \frac{1}{r_b}\frac{\partial}{\partial t}\int_{-\infty}^{0} T\,\mathrm{d}x\right]\right) \tag{9}$$

an apparent initial temperature T_{0a} can be defined to include unsteady energy accumulation in the condensed-phase region

$$T_{0a} \equiv T_0 - \frac{1}{r_b}\frac{\partial}{\partial t}\int_{-\infty}^{0} T\,\mathrm{d}x \tag{10}$$

$$\left.\frac{\partial T}{\partial x}\right|_{0^-,t} \equiv f_s(t) = \frac{r_b}{\alpha_c}(T_s - T_{0a}) \tag{11}$$

[use in place of Eq. (1c)] and the unsteady burning laws can be written as

$$m = m(T_{0a}, P) \tag{12}$$

$$T_s = T_s(T_{0a}, P) \tag{13}$$

The apparent initial temperature T_{0a} has replaced the actual initial temperature T_0 in the steady-state burning laws. These relations are obtained either from a steady model (FM) or steady-state r_b and T_s measurements (ZN). In the case of FM, the solutions generally appear with the two dependent variables m and T_s combined algebraically,

$$F_c(m, T_s; T_{0a}, P) = 0, \qquad F_c(\bar{m}, \bar{T}_s; T_0, \bar{P} = 0) \tag{14}$$

$$F_g(m, T_s; T_{0a}, P) = 0, \qquad F_g(\bar{m}, \bar{T}_s; T_0, \bar{P}) = 0 \tag{15}$$

with one relation, F_c, coming from analysis of the condensed-phase reaction zone and the other, F_g, from the gas-phase reaction zone. When combined with the preceding unsteady differential energy equation, these relations allow solution of the unsteady temperature field in the condensed phase $T(x, t)$ and the unsteady burning rate eigenvalue $m(t)$ for a prescribed unsteady $P(t)$. This solution can be numerical, in which case nonlinear behavior can be simulated, or, in the case of small-amplitude linear behavior, analytic representation is possible. The linear analytic solution is more commonly reported; nonlinear simulations have not been reported much outside of the Russian literature. To summarize, the nonlinear problem consists of solving Eqs. (1), (11), and (12) and (13) or (14) and (15).

Linearized Combustion Model

In the linear approximation, an analytical solution of the QSHOD problem can be obtained. Consider the case of oscillatory burning and, more specifically, the burning response to a harmonic input. The input is a sine wave with circular frequency ω ($=2\pi f$) and amplitude Δp:

$$P(t) = \bar{P} + \mathrm{Re}\{P'(t)\} = \bar{P} + \mathrm{Re}\{\Delta P \exp(i\omega t)\} \tag{16}$$

For a linear response, the corresponding mass flux response and temperature field will also be harmonic at the same frequency

$$m(t) = \bar{m} + \mathrm{Re}\{m'(t)\} = \bar{m} + \mathrm{Re}\{\Delta m \exp[i(\omega t + \Theta)]\} \tag{17}$$

$$R_p = (m'/\bar{m}/P'/\bar{P}) = (\Delta m/\bar{m}/\Delta P/\bar{P})\exp(i\Theta)$$

$$\mathrm{Re}\{R_p\} = |R_p|\cos\Theta \tag{18}$$

$$T(x, t) = \bar{T}(x) + \mathrm{Re}\{T'(x, t)\} = \bar{T}(x) + \mathrm{Re}(\Delta T(x)\exp\{i[\omega t + \varphi(x)]\}) \tag{19}$$

In the linear approximation, we assume $\Delta m \ll \bar{m}$ and $\Delta T \ll \bar{T}$; nonlinear terms such as $m'\partial T'/\partial x$ are negligible. This allows analytic solutions of Eq. (1) to be obtained.

The steady-state solution is

$$(\bar{T} - T_0)/(T_s - T_0) = \exp(x/x_c), \qquad x_c = \alpha_c/\bar{r}_b \tag{20}$$

This equation defines an exponential temperature profile in the inert preheat zone that has a characteristic length scale x_c.

The oscillatory solution, as in the nonlinear case, relies on the steady-state mass flux and surface temperature laws, Eqs. (2) and (3), and the integral energy equation (4). The solution is best obtained using Jacobian transformations.[15–17] The important practical result is that in the linear case the steady-state information appears as sensitivity parameters, that is, the partial derivatives of Eqs. (2) and (3): k, r, ν, and δ (see Nomenclature). The oscillatory solution for pressure-perturbed burning with negligible radiant flux[15–17] is

$$R_p = \frac{\nu + \delta(\lambda - 1)}{\lambda r + k/\lambda - (r + k) + 1} = \frac{nAB + n_s(\lambda - 1)}{\lambda + A/\lambda - (1 + A) + AB} \tag{21}$$

The sensitivity parameters can be obtained from the analytic solution of the WSB model as discussed in the next section.

Condensed-Phase Kinetics

One of the simplest reported kinetic schemes that meets the QSHOD requirement of surface pyrolysis and includes formal consideration of the species equation is zero-order, single-step, unimolecular decomposition with large activation energy $E_c(E_c/RT \gg 1)$ and frequency factor A_c. This initial, endothermic, rate-limiting step is presumed to be followed by rapid exothermic

reactions such that the net converted chemical to sensible enthalpy per unit mass in the condensed phase, Q_c, is possibly exothermic ($Q_c > 0$). The solution for this scheme was first obtained by Merzhanov and Dubovitskii in 1959 and applied to energetic materials.[18] In 1970 it was obtained using activation energy asymptotics (AEA) by Lengelle[19] and applied to endothermic polymer degradation. The following form by Ibiricu and Williams, which includes radiation, appeared in 1975 and was also applied to energetic materials.[20] In the present application radiation is neglected,

$$\bar{m}^2 = \frac{A_c \alpha_c \rho_c^2 C R \bar{T}_s^2 \exp(-E_c/R\bar{T}_s)}{E_c[C(\bar{T}_s - T_0) - Q_c/2 - f_r q_r/\bar{m}]} \tag{22}$$

Equation (22) is a particular form for the functionality F_c indicated in Eq. (14). It is written in steady-state form but can be put in unsteady form based on ZN theory [see Eq. (14)] by replacing T_0 with T_{0a} and dropping the overbars,

$$m^2 = \frac{A_c \alpha_c \rho_c^2 C R T_s^2 \exp(-E_c/RT_s)}{E_c[C(T_s - T_{0a}) - Q_c/2 - f_r q_r/m]} \tag{23}$$

Differentiating the general F_c relation [Eq. (14)], with respect to T_0 gives a relation $r(k)$. Similarly, differentiating F_c with respect to pressure gives relations $\mu(\nu)$ and $\delta(\nu, k)$. These relations have been obtained for zero-order decomposition [Eq. (22)] (Ref. 21).

Gas-Phase Kinetics

A single-step, bimolecular reaction is assumed with activation energy E_g, prefactor B_g, and chemical-to-sensible enthalpy per unit mass Q_g. In the limit of a high-activation-energy reaction, the resulting relation for F_g [Eq. (14)] is

$$\bar{m}^2 = \frac{2k_g B_g W^2 C \bar{T}_f^4 \bar{P}^2}{E_g^2 Q_g^2} \exp\left(\frac{-E_g}{R\bar{T}_f}\right)$$

$$\bar{T}_f = T_0 + \frac{1}{C}[Q_c + Q_g], \qquad \frac{E_g}{RT} \gg 1 \tag{24}$$

In reference to its early use in QSHOD analysis by Denison and Baum[22] and Williams's subsequent theoretical defense of its use,[23] this relation is designated here as DBW. The low-activation-energy limit gives

$$\bar{m}^2 = \frac{4\bar{P}^2 k_g B_g W^2}{CR^2} \cdot \frac{1}{(2/\{Q_g/[C(\bar{T}_s - T_0) - Q_c] - 1\} + 1)^2 - 1}$$

$$\frac{E_g}{RT} \ll 1 \tag{25}$$

The low gas-phase activation-energy limit has recently been proposed as giving closer agreement with most experimental observations for HMX and NC/NG than the high-E_g limit.[14,24,25] Equations (24) and (25) play the role of the function F_g denoted in Eq. (15). They can be differentiated and solved simultaneously with the results from F_c to obtain analytic expressions for the sensitivity parameters.[17] This allows calculation of the linear QSHOD response using fundamental material properties, kinetic ($E_{c,g}$), thermochemical ($Q_{c,g}$), and thermophysical ($C, k_{c,g}$), and environmental parameters (T_0, P). The combination of Eqs. (22) and (25) is referred to here as the WSB model. Combustion parameters representative of homogeneous energetic material were assumed as shown in Table 1.

Chamber Mass Balance

The mass balance on the gas in the chamber is

$$\frac{V}{RT_f}\frac{dP}{dt} = \rho_c r_b A_b - C_d A_t P \tag{26a}$$

$$L^* A' \frac{dP}{dt} = \rho_c r_b \frac{1}{C_d}\frac{A_b}{A_t} - P \tag{26b}$$

$$L^* = \frac{V}{A_t}, \qquad A' = \frac{1}{RT_f C_d}, \qquad \tau_{ch} = A' L^* \tag{26c}$$

Table 1 Input parameters

Parameter	Value
Condensed-phase parameters for propellant	
A_c, 1/s	1.0e17
E_c, cal/mol	40,262.0
Q_c, cal/g	42.0
α_c, cm^2/s	8.0e−4
C, cal/g · K	0.300
ρ_c, g/cm^3	1.6
Gas-phase parameters for propellant and chamber	
B_g, cal^2/cm^3 · atm^2 · g · s · K^2	1.66e−3
E_g, cal/mol	0
Q_g, cal/g	558.0
k_g, cal/cm · s · K	2.0e−4
C, cal/g · K	0.300
W, g/mol	24
T_f, K	2,300
γ (in nozzle C_d)	1.14
A_b/A_t (for 40.18 atm final pressure)	233

where the combustion product temperature T_f is assumed constant. Note that the possible effect of an extended flame zone and even incomplete combustion within the chamber is being neglected here. During the initial low-pressure stage of the pressurization process this assumption may not be satisfied by certain propellants, as noted by Price.[1,2] Note that possible effects due to fluctuating chamber temperature are also ignored. This assumption has been suggested to be reasonable for first-order effects, according to Williams et al.[26] Nevertheless, some studies[27,28] have relaxed this assumption and investigated its effects. One-dimensional, quasi-steady, isentropic flow is assumed in the nozzle to specify the discharge coefficient C_d. The time constant τ_{ch} is the characteristic time for chamber discharge through the nozzle with zero inflow. This equation is coupled through pressure and burning rate to the WSB model. This system of equations is solved numerically by a time-marching, finite difference scheme for $P(t)$ and $r_b(t)$. An initial pressure is assumed. Initial burning rate and solid temperature are set at the steady-state WSB values corresponding to that pressure. The initial state is a relatively low-pressure, steady-state condition that is assumed to exist after the initial flame spreading and ignition transient has passed. This assumption is felt to be reasonable, even though the complex ignition process is not being simulated. The effect of finite-rate flame spreading would be to change the effective initial pressure, perhaps to different values at different spatial locations. To summarize, the complete (chamber and combustion) nonlinear model consists of solving Eqs. (1), (11), (14), (15), and (26), with Eqs. (22) and (25) playing the role of Eqs. (14) and (15). The burning rate r_b is calculated to convergence of less than 0.1% relative error during every time step. The chamber pressure is calculated to convergence of less than 1% relative error.

Linear, Oscillatory Solution for Low L^*

Linearization of the chamber mass balance equation[1] can be accomplished by assuming an exponentially growing or decaying harmonic solution of the form

$$\mathrm{Re}\{P'(t)\} = \Delta P \cos\omega t = P_0 \exp(\alpha t)\cos\omega t \tag{27}$$

$$\mathrm{Re}\{m'(t)\} = \Delta m \cos(\omega t + \Theta) = m_0 \exp(\alpha t)\cos(\omega t + \Theta)$$

$$= |R_p|(\bar{m}/\bar{P})P_0 \exp(\alpha t)\cos(\omega t + \Theta) \tag{28}$$

which leads to the following relations:

$$\omega = |R_p| \sin\Theta/\tau_{ch} \tag{29}$$

$$\alpha = (|R_p|\cos\Theta - 1)/\tau_{ch} \tag{30}$$

For a physically realistic oscillatory solution, the frequency determined by Eq. (29) must be positive, and in addition for a spontaneous oscillation to grow, the growth constant determined by Eq. (30) must

also be positive ($\alpha > 0$). These conditions place upper and lower frequency constraints, corresponding to $\mathrm{Im}\{R_p\} > 0$ ($\Theta > 0$) and $\mathrm{Re}\{R_p\} > 1$, respectively. The stability limit is defined by the condition $\alpha = 0$, and corresponding properties are designated by a zero subscript, such as L_0^*, f_0, Ω_0, R_{p0}, etc. Setting $\alpha = 0$ in Eqs. (29) and (30) and solving for L_0^* gives

$$L_0^* \approx \left(\alpha_c \Big/ A' \bar{r}_b^2\right)\left(\sqrt{|R_{p0}|^2 - 1}\Big/\Omega_0\right) \propto 1/\bar{P}^{2n} \qquad (31)$$

Results and Discussion

Small Pressure Changes (Linear Behavior)

Linear conditions were simulated first to help validate the numerical solution, using the analytic solution discussed earlier, and to locate the linear stability boundary. Figure 2 shows the linear frequency-response function calculated according to Eqs. (21), (22), and (25) for the base case of $P = 40.18$ atm (the otherwise unnecessary precision of this number is to distinguish it from the initial pressure of 40.00 used for linear calculations). See Table 1 for propellant parameters. For reference, the sensitivity parameters at this pressure are $\nu = 0.89$, $k = 0.98$, $r = 0.044$, and $\delta = -0.066$. Only the phase lead portion of the response function is shown in Fig. 2 because, by Eq. (29), only for $\sin\Theta > 0$ is there the possibility of oscillatory solutions ($f > 0$). Figure 3 shows the L^* vs frequency values calculated from Eq. (29) and α vs frequency from Eq. (30). It can be seen that for this response function, L^* is a single-valued function of frequency. (Price[1] has noted the interesting theoretical possibility of L^* being a multiple-valued function of frequency.)

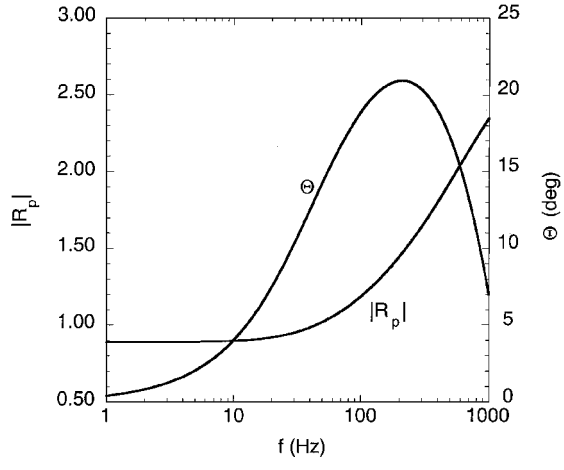

Fig. 2 Linear frequency-response function for propellant parameters in Table 1 at 40.18 atm.

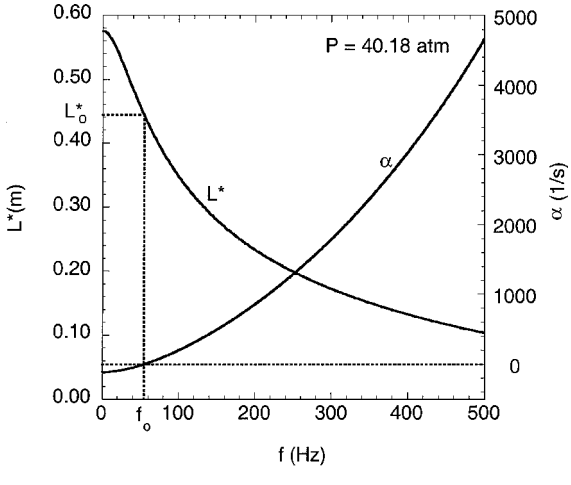

Fig. 3 Linear L^* parameters (L^* and growth constant) for response function of Fig. 2 (40.18 atm); linear stability limit occurs at $f_0 = 54$ Hz with $L_0^* = 0.444$ m.

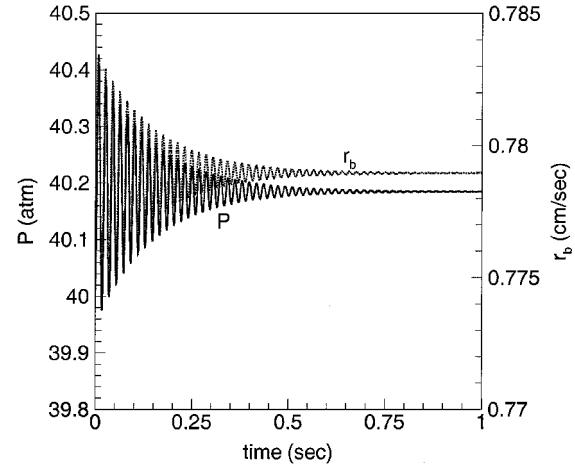

Fig. 4 Linearly stable case, $L^* = 0.450$ m (constant), $\alpha = -6.74$ 1/s, initial pressure 40.00 atm, final pressure 40.18 atm ($L_0^* = 0.444$ m); see Fig. 1a.

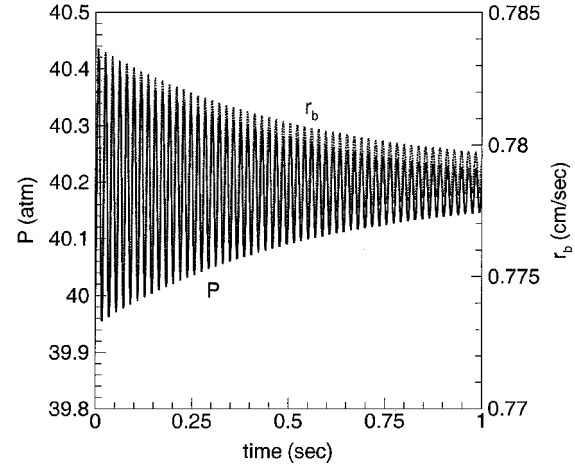

Fig. 5 Linearly stable case, $L^* = 0.445$ m (constant), $\alpha = -1.85$ 1/s, initial pressure 40.00 atm, final pressure 40.18 atm ($L_0^* = 0.444$ m); see Fig. 1a.

The linear stability boundary is located at $\alpha = 0$, where $f = 54$ Hz and $L^* = 0.444$ m. This value of L^* (where $\alpha = 0$) is referred to as L_0^* and the corresponding frequency f_0.

Figures 4 and 5 show pressure and burning-rate histories for an initial pressure of 40 atm and two different L^* values, both slightly above L_0^* ($\alpha < 0$). The burning surface area, nozzle throat area, combustion parameters, motor parameters, and other parameters are such that the final equilibrium pressure is only slightly higher, 40.18 atm. Therefore, due to the small magnitude of pressure change involved, the system behavior is linear, at least initially.

Figure 4 shows a case for a constant value of $L^* = 0.450$ m (imagine an end-burning configuration with the propellant being fed into the chamber at a rate equal to its consumption rate). Because this value of L^* is greater than L_0^*, the linear growth/decay constant α is negative. The system oscillates with amplitude decaying to the final steady-state conditions. A curve fit of the numerical results gives $\alpha = -6.74$ 1/s, whereas the linear analytic solution gives -8.27 1/s. The numerical frequency is 54 Hz, whereas that predicted by the linear analytic theory is 52 Hz. This is an example of a system that is linearly stable, that is, stable to small perturbations. It corresponds to the type of stable, steady burning behavior shown in Fig. 1a (see also Fig. 6a of Ref. 1, high-L^* behavior).

Figure 5 shows a case for a slightly smaller L^* value, 0.445 m (L^* still being kept constant for the calculation). Because the condition $L^* > L_0^*$ still holds, the corresponding α value is still negative (-1.85 1/s) but closer to zero than in the preceding case. Thus, the system is closer to the linear stability boundary, and the

oscillation decay time is longer. Still the system approaches the expected steady-state burning condition. The numerical and analytical frequencies for this case are both 54 Hz.

Figure 6 shows a case for even smaller L^*, 0.431 m, such that L^* is now less than the value for linear stability, $L^* < L_0^*$, and the growth constant is positive (15.2 1/s). The oscillation amplitude grows until nonlinear effects take over, and the burning rate suddenly goes to zero; the propellant extinguishes. This is an example of a system that is linearly unstable being perturbed by a small perturbation, becoming nonlinear, and finally extinguishing. This case corresponds to the type of experimentally observed behavior shown in Fig. 1c (see also Ref. 1, Figs. 1 and 6c). Figure 6 also shows how burning rate leads pressure during L^* oscillations, in agreement with the positive phase (16 deg) of Fig. 2 at 56 Hz. The reason the burning rate goes to zero instead of blowing up is discussed later, when the effect of pressure on linear stability properties is considered.

Figure 7 shows what can happen if the increase in L^* corresponding to propellant consumption is taken into account rather than assuming L^* is constant. In this case rather than feeding the propellant into an end burner at the linear regression rate to maintain constant volume, the volume increases at a rate equal and opposite to the propellant volumetric consumption rate. The simulation begins at $L^* = 0.365$, which is less than the critical value for linear stability ($L_0^* = 0.444$). The oscillations initially grow in amplitude. However, because L^* crosses the stability boundary at around 0.045 s, the growth in amplitude is reversed into a decay. This case corresponds to the type of experimentally observed behavior shown in

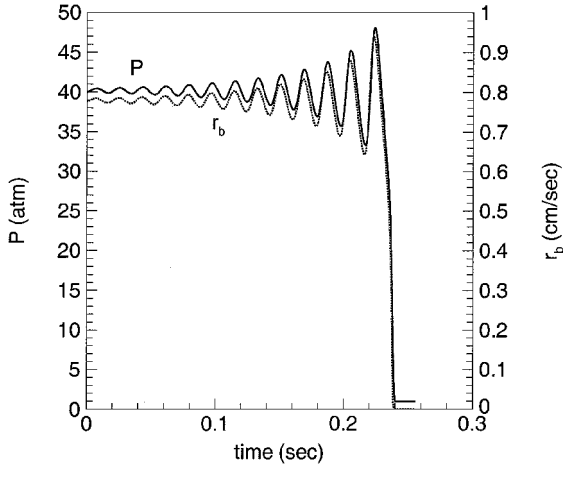

Fig. 6 Linearly unstable case, $L^* = 0.431$ m (constant), $\alpha = 15.2$ 1/s, initial pressure 40.00 atm, final pressure 40.18 atm ($L_0^* = 0.444$ m), leading to extinction; see Fig. 1c.

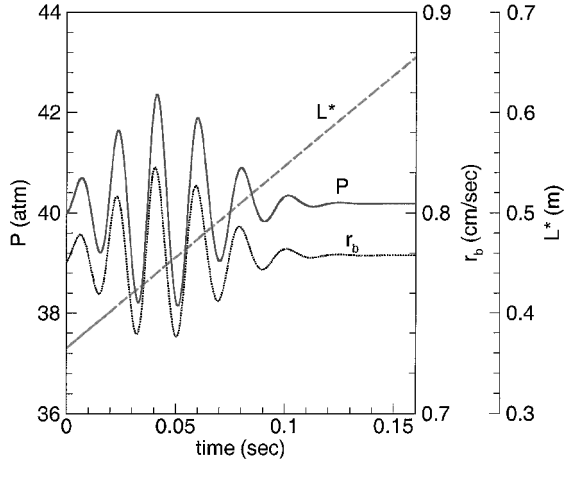

Fig. 7 Variable L^* case, initially linearly unstable ($L^* = 0.365$ m), becomes stable due to increase in L^* (final $L^* = 0.909$); Initial pressure 40.00 atm, final pressure 40.18 atm ($L_0^* = 0.444$ m); see Fig. 1b.

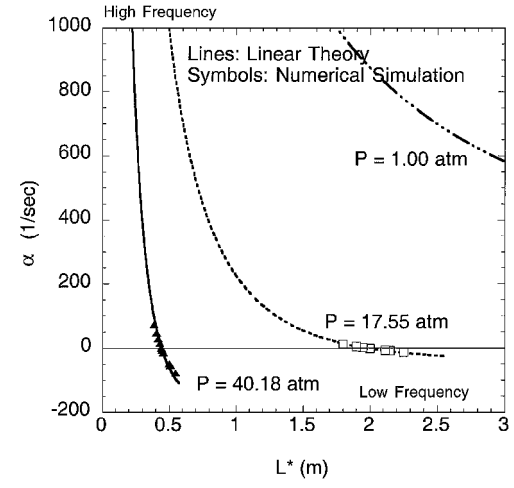

Fig. 8 Effect of pressure on linear stability parameters α vs L^* for propellant parameters in Table 1: stability boundary at $\alpha = 0$; curve for 40.18 atm corresponds to Fig. 3.

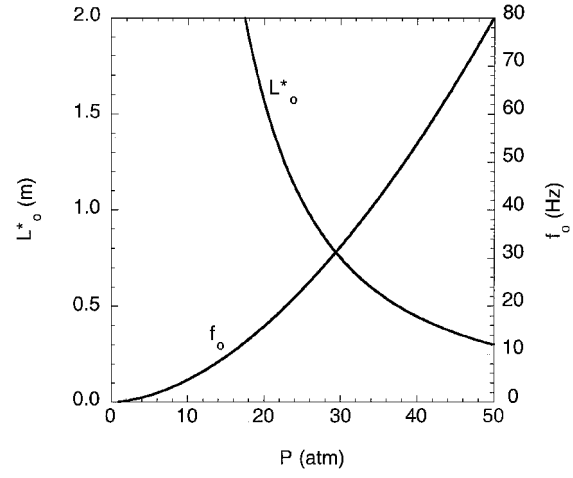

Fig. 9 Linear stability boundary for propellant parameters in Table 1: stable for $L^* > L_0^*$ ($\alpha < 0$); unstable for $L^* < L_0^*$ ($\alpha > 0$).

Fig. 1b (see also Ref. 1, Figs. 3 and 6b). All of the cases described are for linear behavior about a pressure of 40 atm.

Figures 8 and 9 show the effect of varying pressure on linear oscillatory L^* behavior. Figure 8 shows α plotted as a function of L^* for three pressures, 40.18, 17.55, and 1.0 atm [this type of plot can be generated from Fig. 3 or Eqs. (29) and (30) by eliminating frequency]. Near the linear stability boundary ($\alpha = 0$), the numerical and linear analytical solutions agree well, as expected, thus validating the numerical computations for these conditions. The value of L^* at the stability boundary, L_0^*, is a decreasing function of pressure. For low pressures, the α vs L^* curves intersect $\alpha = 0$ at high values of L^* and with a more gradual slope. Thus, the range of L^* values over which oscillatory behavior may be observed widens as pressure decreases, which partly accounts for oscillatory bulk-mode instability appearing more often at lower pressures. Figure 9 shows the locus of intersection points from Fig. 8 (L_0^* and corresponding frequency f_0) as a function of pressure. The reason for this effect of pressure on L_0^* is the effect burning rate has on the thickness of the heated layer at the surface of the solid, $x_c = \alpha_c / r_b$. As pressure increases, the time for burnoff of this layer, $t_c = x_c / r_b$, decreases as $1/r_b^2$. As a result, the $1/r_b^2$ scaling also appears in the nondimensional frequency Ω. Using this scaling in Eqs. (29) and (30) (with $\alpha = 0$) gives Eq. (31). The latter proportionality in Eq. (31) assumes that the response R_p as a function of nondimensional frequency is independent of pressure, which implies that the steady-state sensitivity parameters are also independent of pressure. Although this is not true strictly, it is a reasonable approximation for the purpose of

estimating the effect of pressure on L_0^*. Thus, as shown in Eq. (31), L_0^* varies approximately inversely with pressure to the power of $2n$.

What is the implication of the pressure trend shown in Figs. 8 and 9 for motor behavior? During motor firing, the initial pressure is well below the final target operating pressure. As the motor firing proceeds and the motor pressurizes, L_0^* decreases. At the same time, the actual motor L^* value increases. The instantaneous values of L^* and L_0^* determine the state of linear stability of the motor at any given time. Thus, the relative magnitudes of L^* and L_0^* give some indication of how the motor will behave but not a complete description because L_0^* is only a linear concept. With regard to the actual (nonlinear) stability behavior of the motor, not only the instantaneous values but also the relative rates of increase for L^* and decrease for L_0^* are probably important. Motor behavior under more realistic nonlinear dynamic conditions is considered next.

Large Pressure Changes (Nonlinear Behavior)

In the next set of simulations, nonlinear behavior is ensured by an increase in the magnitude of the imposed pressure change. The initial pressure is reduced, in most cases to 1.0 atm, while propellant combustion and chamber conditions are kept the same such that the final equilibrium pressure (assuming extinction does not occur) is still 40.18 atm. Constant L^* is maintained during the burn (propellant fed into an end burner). Because the mean pressure now changes significantly during the course of the burn, the linear stability properties, that is, α, L_0^*, etc., also change. At 1 atm, the value of L_0^* is 353 m, one or two orders of magnitude above the initial L^* value in most practical systems. (Typical initial L^* values range from 2 to 30 m.) Therefore, as shown in Fig. 8, the initial (1 atm) α value is positive and very large for typical L^* values. When pressurization begins, the motor is in a very unstable state. However, as it pressurizes, it moves toward more stable parameter space: L^* increases and L_0^* and α decrease (see Fig. 8). How the motor will behave depends on the initial value of L^*, the initial pressure, the final target pressure, and other conditions. Various cases illustrating different types of motor behavior are considered next.

Figure 10 shows a case for a very small value of $L^* = 0.093$ m (constant). Even at the final target pressure of 40.18 atm, $L_0^* = 0.444$ m is still much larger than the initial L^* value and α is positive and very large (5570 1/s). Because according to linear analysis the target final state is not stable, it can be anticipated that the motor will not be able to reach a steady burning condition at the target pressure. Figure 10 bears out this prediction. From the initial state at 1 atm, the pressure begins to rise rapidly and in the process L_0^* and α decrease. As indicated by Figs. 8 and 9, the effect of raising pressure is to make the system more stable. Eventually, after reaching 525 atm, the pressure begins decreasing. As pressure decreases, the system becomes less stable according to linear theory (Figs. 8 and 9). There is a brief pause in the pressure decent at about 70 atm, and then the propellant extinguishes. These same stabilizing/destabilizing influences correlating with increasing/decreasing pressure are also evident in Fig. 6, where the system became nonlinearly unstable during negative dP/dt, not positive. Note that whereas this observation seems to hold for the propellant parameters under consideration (which includes $n < 1$), it may not hold for other propellant conditions.

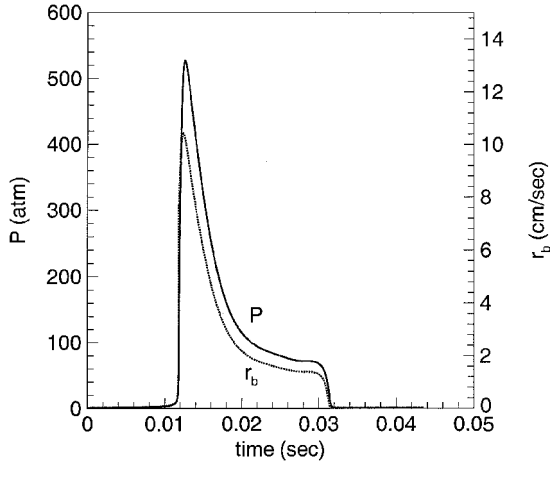

Fig. 10 Nonlinear case (linearly unstable) leading to extinction (possible chuffing); $L^* = 0.093$ m (constant), initial pressure 1.00 atm, final target pressure 40.18 atm ($L_0^* = 0.444$ m, $\alpha = 5570$ 1/s); see Fig. 1d.

The case shown in Fig. 10 is similar to experimentally observed behavior for small L^* values as shown in Fig. 1d and as described in Ref. 1 (Fig. 6e). Experimentally it is often observed that the propellant reignites and repeats the cycle. (Extinction, which follows oscillatory instability as shown in Figs. 6 and 1c, can also be followed by reignition and repetition of the cycle, or chuffing.) The process of reignition can not be simulated in the present model because the ignition process itself is not simulated, but presumably it might be with the inclusion of an ignition model. Note that the L^* value of 0.093 m may seem unrealistically small in light of the fact that self-quenching is usually observed experimentally at much bigger L^* values. However, those observations are usually at much lower pressures than this calculation. As final target pressure is reduced, self-quenching is exhibited at higher L^* values. It should also be reiterated that the pressure in Fig. 10 exhibits a severe excursion (>500 atm) above the final target pressure (40.18 atm). The severity of the pressure excursion is partly due to the very small initial L^* value. However, this type of overpressurization also happens even for larger L^* values, as discussed next.

Figure 11 shows a case with a larger value of $L^* = 2.6$ m (constant), a value typical of low port-to-throat area grains. This L^* value is big enough that at 40 atm no linear oscillatory solution exists (see Fig. 3). At 1 atm, a solution does exist, and the α value is positive and large (673 1/s), which causes the pressure initially to

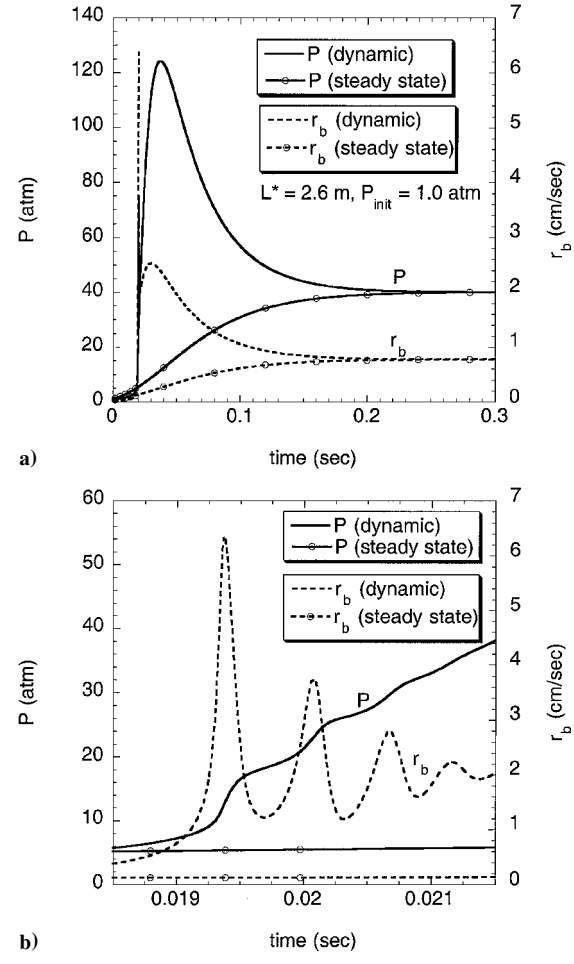

Fig. 11 Nonlinear case: exhibiting initial pressurization spike, $L^* = 2.6$ m (constant), initial state linearly unstable; final state linearly stable. Initial high-frequency oscillation magnified in b). Fully quasi-static calculation (including solid) labeled steady state.

rise rapidly. The interesting feature is the severity of the overpressurization spike (>120 atm). Similar initial pressurization spikes have been commonly attributed to igniter mass flux and/or erosive burning[29–34] (see Fig. 2.15 of Ref. 29, Fig. 4.17 of Ref. 30, Fig. 6 of Ref. 32, Fig. 1 of Ref. 33, and Fig. 4 of Ref. 34). However, the calculations of Fig. 11 include no such effects, only nonlinear bulk-mode chamber mass conservation and combustion. Propellant grains that would be considered conducive to erosive burning (small port-to-throat area ratios and large length-to-diameter ratios) would also be conducive to low-L^* or dP/dt nonlinear dynamic burning effects. Therefore, separating these effects in motor pressure data is difficult. The relative importance of erosive burning and dynamic burning in causing the initial pressurization spike appears to be an unresolved issue at this time. Some studies[29–34] suggest that erosive burning is more important. At least one paper has proposed a dynamic burning explanation of the ignition spike.[27] That study used a linearized dP/dt burning model, not a nonlinear dynamic burning model. In addition, a variable gas temperature feature was assumed. According to Williams et al.,[26] if the variable gas temperature effect was not assumed, that is, isothermal gas, the pressure spike went away. In the present simulations constant gas temperature has been assumed (a reasonable representation of the energy equation for capturing first-order effects, according to Williams et al.[26]), and the pressure spike is retained. The present simulations suggest that dynamic burning should be given more consideration in explaining anomalous initial pressurization spikes, as well as depressurization transients. With respect to the latter, Williams et al.[26] have commented that "erosion effects certainly do not explain all of the experimental results since such a burning rate increase has been observed with end-burning grains, on which erosion effects are likely to be negligible."

The burning rate and pressure calculated using the steady-state burning laws are also shown in Fig. 11 for comparison and to illustrate the significance of the nonlinear dynamic burning effect. This calculation assumes completely quasi-static combustion, including the solid phase (effectively equivalent to $r_b = aP^n$, although the WSB equations are actually used). Figure 11 shows that the quasi-static pressure reaches the equilibrium pressure at about the same time as the dynamic case (0.25 s) but does so monotonically, without a pressure spike.

Another feature of Fig. 11 is a high-frequency oscillation that occurs early in the burn, at about $t = 0.01$ s. The expanded timescale plot of Fig. 11b resolves this region more clearly. The characteristic frequency of this oscillation (about 1500 Hz) matches the inert condensed-phase heated layer characteristic frequency r_b^2/α, suggesting that this is an intrinsic instability related to the propellant combustion and may or may not be coupled to the chamber gasdynamics. Although the burning-rate amplitude of this oscillation is quite large relative to the mean, the frequency is high. The combined effect is such that the pressure oscillation amplitude is only of the same order as the mean pressure or less. This type of oscillation appears not to have been reported experimentally and indeed would be difficult to detect through the usual method of pressure measurement unless the pressure amplitude became larger.

Figure 12 shows how significant the dynamic burning effect can be even for larger values of L^*, typical of large boosters. For $L^* = 20$ m, Fig. 12 shows that although the initial overpressurization spike is gone, the rate of pressurization is still much greater with dynamic burning than for the fully quasi-static (steady-state) case. This suggests that the rapid pressurization rate in most solid rockets is at least partly due to the inherent L^* instability of the initial state, where $L^* < L_0^*$ ($\alpha > 0$). This condition ($L^* < L_0^*$) is not so much due to the value of L^* as it is to the inherently large values of L_0^* at low pressures, as shown in Fig. 9. This effect can also be seen in Fig. 1a where, although L^* is big, there is evidence of a weak pressure spike.

Figure 13 shows the effect of initial pressure using a set of cases for the same (constant) L^* value (0.445) that was used in the linear results of Fig. 5 (which had an initial pressure of 40 atm). This L^* value is just slightly above the stability value (0.444) based on the final target pressure of 40.18 atm such that at the final target pressure the system is linearly stable, barely. In Fig. 12, much lower initial

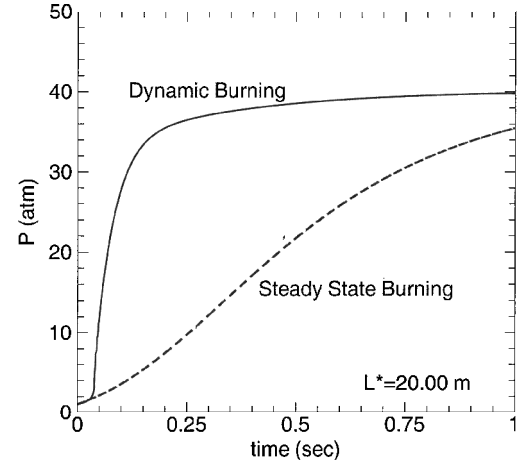

Fig. 12 Nonlinear case: exhibiting rapid initial pressurization rate, dynamic burning effect, $L^* = 20$ m (constant); initial state linearly unstable; final state linearly stable. Fully quasi-static calculation (including solid) labeled steady state.

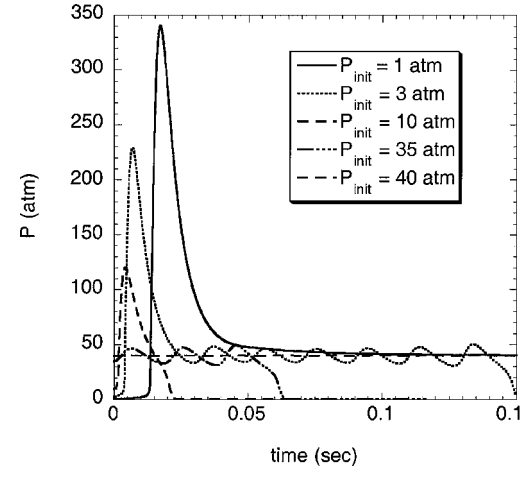

Fig. 13 Nonlinear case: effect of initial pressure, $L^* = 0.445$ m (constant); final target pressure 40.18 atm ($L_0^* = 0.444$ m). High and low initial pressures go to stable burning state and intermediate initial pressures extinguish.

pressures are considered than in Fig. 5. The initial pressures of 1.0, 3.0, and 10.0 atm are each low enough that the initial α values are all positive and quite large. The results show that starting at 1 atm the pressure goes through a severe spike, reaching 340 atm, before stabilizing to the final pressure. The pressure never falls below the critical value ($P > P_0 = 40.13$ atm) and, therefore, α remains negative, and the solution remains nonoscillatory. For the next initial pressure, 3 atm, a 230-atm spike is followed by a marginally stable oscillatory period and then by extinction. The oscillatory period exhibits distinctly nonlinear (anharmonic) waveform and has the appearance of a limit cycle with nearly constant amplitude. Because the pressure is able to fall below the critical value after the initial spike, α becomes positive, and the pressure begins to oscillate. For the 10-atm initial condition, the pressure peaks at 120 atm followed almost immediately by extinction. In this case, even though α becomes positive after P falls below P_0, the rate of pressure drop is too great (a nonlinear effect) for the pressure to begin to oscillate. At 35-atm initial condition, the pressure oscillates for three cycles before extinction. The magnitude of the first maximum is reduced to the same order as the subsequent oscillations. At 40-atm initial condition, the system is stable (see also Fig. 5). The pressure oscillates at the same frequency (54 Hz) but the amplitude is too small to appear on the scale of Fig. 13. The effect of initial pressure on long-term stability of the system, that is, does it extinguish or not,

is clearly nonmonotonic, because at 40-atm initial pressure (Fig. 5), the system, though oscillatory, continues to burn as long as there is propellant. Between 10 and 35 atm initial condition, the pressure spike of the intermediate-initial-pressure, nonoscillatory, extinction regime turns into the first oscillation of the high-initial-pressure, oscillatory regime. At about 38-atm initial pressure and above, the system is able to continue burning to a stable final state.

Dual-frequency oscillation is a phenomenon that has been reported experimentally and discussed theoretically, at least in a preliminary way. Price's[1,2] adaptation of the linear theory is probably the most developed explanation of such observations. As noted earlier Price suggested multiple values of frequency for a single L^* value resulting as an intrinsic property of the linear-response function. Another idea that has been suggested is two-stage flame structure.[6,7] It also may be that, as Price as suggested,[1,2] there are multiple dual-frequency mechanisms. We have also observed several numerical results that appear to have a dual-frequency nature; therefore, brief comments are made on those. The most common type of a dual-frequency behavior for the propellant parameters of this study is that manifested in the burning rate of Fig. 11. It is not uncommon in cases that have a strong initial pressurization spike for the burning rate to exhibit a few cycles of high-frequency oscillation during the positive dP/dt portion of the pressure spike. In some cases, the amplitude of these burning-rate oscillations is large enough to produce noticeable oscillations in pressure. The frequency of these oscillations seems to be well above any characteristic linear L^* frequency. It seems rather to correspond to the characteristic thermal relaxation frequency of the heated layer at the surface of the solid. Sometimes the initial high-frequency oscillation (and spike) is followed by a low-frequency, L^* oscillation, as in Fig. 13 for 3-atm initial pressure.

Figure 14 shows another example of a high-frequency burning-rate oscillation occurring during the positive dP/dt portion of the initial pressurization spike. In this case the high-frequency oscillation is strong enough to produce noticeable oscillations in pressure. The results of Fig. 14 are obtained by modifying the propellant combustion parameters through shifting 8 cal/g of heat release from the gas phase to the condensed phase. The initial and target final pressures are 1 and 12 atm, respectively. By making other adjustments to the propellant combustion parameters, we have also found it possible to create response functions with multiple values of frequency for a single L^* value, as suggested by Price.[1,2] In turn these response functions are capable of generating dual-frequency oscillatory pressure–time histories. Whether any of these theoretical dual-frequency mechanisms can be shown conclusively to correspond to experimental observations remains to be seen. Certainly dual-frequency behavior needs further systematic evaluation. However, it does seem that nonlinear dynamic L^* combustion is another potential cause to be considered for dual-frequency oscillations.

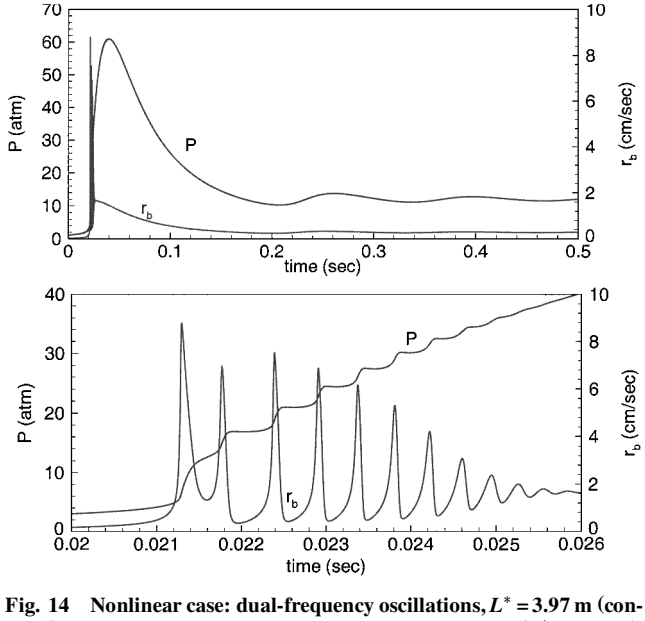

Fig. 14 Nonlinear case: dual-frequency oscillations, $L^* = 3.97$ m (constant); initial pressure 1.0 atm; final pressure 12.05 atm ($L_0^* = 3.74$ m). Propellant properties same as Table 1 except $Q_c = 50$ and $Q_g = 550$ cal/g.

Summary and Conclusions

Nonlinear combustion behavior has been investigated using a new nonlinear combustion model (WSB) in a simple bulk-mode combustor. Simulated behavior resembles experimental trends observed at low pressures for different values of L^* as noted by Price.[1,2] At large values of L^* (see Fig. 1a), normal steady burning is obtained; perturbations are damped ($\alpha < 0$). For smaller values of L^*, sustained oscillatory burning can occur and perturbations can grow ($\alpha > 0$). If L^* increases fast enough as a result of propellant consumption, the system may revert back to the linearly stable domain with the effect that the oscillations cease to grow and instead decay (Fig. 1b). If L^* does not increase fast enough as a result of propellant consumption (relative to how large α was to begin with), the oscillations will grow large in amplitude and be followed by extinction of burning (Fig. 1c). For still smaller values of L^*, the growth constant α will be so large that quenching will occur on the first cycle, usually soon after a large pressure spike (Fig. 1d). The results confirm that the range of L^* values for achieving oscillatory behavior is relatively narrow, becoming more so as pressure increases. For most operating pressures, bulk-mode oscillation occurs only at relatively small values of L^* and then only over very narrow ranges of L^*. The rate of change of L^* in the motor would normally be so fast that oscillatory motion would not be manifested (Figs. 1e and 1f). This has led to the (correct) perception that oscillatory bulk-mode instability is only a problem under limited conditions, that is, low pressure and low L^*. However, it may be that an important high-pressure, low-L^* phenomenon has gone largely unrecognized. The present computations have shown that even at moderate and high pressures, if L^* is low enough, a large initial pressurization spike occurs. The values of L^* involved (2–3 m) are typical of test motors in which ignition spikes have been observed. This suggests that initial pressurization spikes often attributed to erosive burning or igniter mass flux may be primarily due to nonlinear combustor dynamics at low L^*. Even in the absence of a pressurization spike, these results suggest that L^* instability or nonlinear dynamic burning associated with a large, positive initial value of α contributes to rapid pressurization in many motors. Exploratory calculations with reduced burning-rate pressure sensitivity, more typical of composite propellants, have also exhibited overpressurization; this will be reported in future.

Acknowledgments

Funding for this work by the U.S. Department of Energy (University of Illinois at Urbana–Champaign–Accelerated Strategic Computing Initiative Center for Advanced Simulation of Rockets) through the University of California under Subcontract B341494 and the Office of Naval Research and Ballistic Missile Defense Organization (N00014-1-95-1339) is gratefully acknowledged.

References

[1] Price, E. W., "L^* Instability," *Nonsteady Burning and Combustion Stability of Solid Propellants*, edited by L. De Luca, E. W. Price, and M. Summerfield, Vol. 143, Progress in Astronautics and Aeronautics, AIAA, Washington, DC, 1992, Chap. 9, pp. 325–361.

[2] Price, E. W., "Experimental Combustion Instability," *Fundamentals of Solid Propellant Combustion*, edited by K. K. Kuo and M. Summerfield, Vol. 90, Progress in Astronautics and Aeronautics, AIAA, New York, 1984, Chap. 13, pp. 733–790.

[3] Barrere, M., "Introduction to Nonsteady Burning and Combustion Instability," *Nonsteady Burning and Combustion Stability of Solid Propellants*, edited by L. De Luca, E. W. Price, and M. Summerfield, Vol. 143, Progress in Astronautics and Aeronautics, AIAA, Washington, DC, 1992, Chap. 1, pp. 17–58.

[4] Tanaka, M., and Nakaji, K., "An Experimental Study on Low-Frequency Combustion Instability of Composite Propellants," AIAA Paper 98-3552, July 1998.

[5] Sehgal, R., and Strand, L., "A Theory of Low-Frequency Combustion Instability in Solid Rocket Motors," *AIAA Journal*, Vol. 2, No. 4, 1964, pp. 696–702.

[6]Schoyer, H. F. R., and de Bont, R. T. M., "Experimental Verification of Temperature Fluctuations During Combustion Instability," *AIAA Journal*, Vol. 24, No. 2, 1986, pp. 340, 341.

[7]Schoyer, H. F. R., "Incomplete Combustion: A Possible Cause of Combustion Instability," *AIAA Journal*, Vol. 21, No. 8, 1983, pp. 1119–1126.

[8]Schoyer, H. F. R., "Results of Experimental Investigations of the L^* Phenomenon," *Journal of Spacecraft and Rockets*, Vol. 17, No. 3, 1980, pp. 200–207.

[9]Schoyer, H. F. R., "L^* Oscillation and a Pressure Frequency Correlation for Solid Rocket Propellants," *AIAA Journal*, Vol. 15, No. 9, 1977, pp. 1347, 1348.

[10]Boggs, T. L., and Beckstead, M. W., "Failure of Existing Theories to Correlate Experimental Nonacoustic Combustion Instability Data," *AIAA Journal*, Vol. 8, No. 4, 1970, pp. 626–631.

[11]Cheng, S. I., "L^*-Combustion Instability in Solid Propellant Rocket Combustion," *Recent Advances in the Aerospace Sciences*, edited by C. Casci, Plenum, New York, 1985, Chap. 13, pp. 257–278.

[12]De Boer, R. S., Schoyer, H. F. R., and Wolff, H., "Results of L^*-Instability Experiments with Double Base Rocket Propellants II," Dept. of Aerospace Engineering, Rept. LR-252, Delft Univ. of Technology, Delft, The Netherlands, 1977.

[13]Coates, R. L., Cohen, N. S., and Harvill, L. R., "An Interpretation of L^* Combustion Instability in Terms of Acoustic Instability Theory," *AIAA Journal*, Vol. 5, No. 6, 1967, pp. 1097–1102.

[14]Ward, M. J., Son, S. F., and Brewster, M. Q., "Role of Gas- and Condensed-Phase Kinetics in Burning Rate Control of Energetic Solids," *Combustion Theory and Modeling*, Vol. 2, 1998, pp. 293–312.

[15]Novozhilov, B. V., *Nonstationary Combustion of Solid Propellants*, Nauka, Moscow, 1973; English translation available from National Technical Information Service, NTIS No. AD-767 945, 1973.

[16]Novozhilov, B. V., "Theory of Nonsteady Burning and Combustion Stability of Solid Propellants by the Zeldovich–Novozhilov Method," *Nonsteady Burning and Combustion Stability of Solid Propellants*, edited by L. De Luca, E. W. Price, and M. Summerfield, Vol. 143, Progress in Astronautics and Aeronautics, AIAA, Washington, DC, 1992, Chap. 15, pp. 601–641.

[17]Son, S. F., and Brewster, M. Q., "Linear Burning Rate Dynamics of Solids Subjected to Pressure or External Radiant Flux Oscillations," *Journal of Propulsion and Power*, Vol. 9, No. 2, 1993, pp. 222–232.

[18]Merzhanov, A. G., and Dubovitskii, F. I., "The Theory of Stationary Combustion in Powder," *Proceedings of the USSR Academy of Science*, Vol. 129, No. 1, 1959, pp. 153–156.

[19]Lengelle, G., "Thermal Degradation Kinetics and Surface Pyrolysis of Vinyl Polymers," *AIAA Journal*, Vol. 8, No. 11, 1970, pp. 1989–1996.

[20]Ibiricu, M. M., and Williams, F. A., "Influence of Externally Applied Thermal Radiation on the Burning Rates of Homogeneous Solid Propellants," *Combustion and Flame*, Vol. 24, 1975, pp. 185–198.

[21]Brewster, M. Q., and Son, S. F., "Quasi-Steady Combustion Modeling of Homogeneous Solid Propellants," *Combustion and Flame*, Vol. 103, 1995, pp. 11–26.

[22]Denison, M. R., and Baum, E., "A Simplified Model of Unstable Burning in Solid Propellants," *American Rocket Society Journal*, Vol. 31, No. 8, 1961, pp. 1112–1122.

[23]Williams, F. A., "Quasi-Steady, Gas-Phase Flame Theory in Unsteady Burning of a Homogeneous Solid Propellant," *AIAA Journal*, Vol. 11, No. 9, 1973, pp. 1328–1330.

[24]Ward, M. J., Son, S. F., and Brewster, M. Q., "Steady Deflagration of HMX with Simple Kinetics: A Gas Phase Chain Reaction Model," *Combustion and Flame*, Vol. 114, 1998, pp. 556–568.

[25]Brewster, M. Q., Ward, M. J., and Son, S. F., "Simplified Combustion Modeling of Double Base Propellant: Gas Phase Chain Reaction vs Thermal Decomposition," *Combustion Science and Techology*, Vol. 154, 2000, pp. 1–30.

[26]Williams, F. A., Barrere, M., and Huang, N. C., *Fundamental Aspects of Solid Propellant Rockets*, Technivision Services, Slough, England, U.K., 1969, pp. 529–550.

[27]Paul, B. E., Lovine, R. L., and Fong, L. Y., "A Ballistic Explanation of the Ignition Pressure Peak," AIAA Paper 64-121, Jan. 1964.

[28]Kumar, K. R. A., and Lakshmisha, K. N., "A Computational Study of the L^* Instability with a Nonlinear Frequency Response," *Proceedings of the 5th International Symposium on Special Topics in Chemical Propulsion: Combustion of Energetic Materials* (to be published by Begell House, New York).

[29]Zeller, B., "Solid Propellant Grain Design," *Solid Rocket Propulsion Technology*, edited by A. Davenas, Pergamon, New York, 1993, Chap. 2.

[30]Gossant, B., "Solid Propellant Combustion and Internal Ballistics of Motors," *Solid Rocket Propulsion Technology*, edited by A. Davenas, Pergamon, New York, 1993, Chap. 4.

[31]Adams, D. M., "Igniter Performance in Solid-Propellant Rocket Motors," *Journal of Spacecraft and Rockets*, Vol. 4, No. 8, 1967, pp. 1024–1029.

[32]Kumar, M., and Kuo, K. K., "Flame Spreading and Overall Ignition Transient," *Fundamentals of Solid Propellant Combustion*, edited by K. K. Kuo and M. Summerfield, Vol. 90, Progress in Astronautics and Aeronautics, AIAA, New York, 1984, Chap. 6, pp. 305–341.

[33]Razdan, M. K., and Kuo, K. K., "Erosive Burning of Solid Propellants," *Fundamentals of Solid Propellant Combustion*, edited by K. K. Kuo and M. Summerfield, Vol. 90, Progress in Astronautics and Aeronautics, AIAA, New York, 1984, Chap. 10, pp. 551–590.

[34]Blomshield, F. S., Crump, J. E., Mathes, H. B., Stalnaker, R. A., and Beckstead, M. W., "Stability Testing of Full-Scale Tactical Motors," *Journal of Propulsion and Power*, Vol. 13, No. 3, 1997, pp. 349–355.